# Solution-Based Straight and Branched CdTe Nanowires

Masaru Kuno,*,† Omar Ahmad,† Vladimir Protasenko,† Daniel Bacinello,†,‡ and Thomas H. Kosel§

*Department of Chemistry and Biochemistry, Notre Dame Radiation Laboratory, and Department of Electrical Engineering, University of Notre Dame, Notre Dame, Indiana 46556, and Department of Chemistry, University of Waterloo*

*Received July 6, 2006. Revised Manuscript Received September 16, 2006*

The synthesis, characterization, and optical properties of high quality straight and branched CdTe nanowires (NWs) are described. A solution-based (solution−liquid−solid) approach is used to synthesize the NWs by employing a low melting bimetallic nanoparticle catalyst to induce one-dimensional (1D) growth. This leverages advances in the development of high quality colloidal quantum dots (QDs) with emerging techniques for manufacturing 1D nanomaterials. Resulting straight and branched CdTe NWs have diameters below twice the corresponding bulk exciton Bohr radius and, as a consequence, exhibit confinement effects in their linear absorption. Size distributions range from 15% to 20%, with NW lengths commonly exceeding 10 $\mu$m. Intrawire diameter variations are on the order of 5%. High-resolution transmission electron microscopy (TEM) images reveal that the wires are crystalline and grow exclusively along the <111> and <0001> directions of the corresponding zincblende and wurtzite phases. Branched NW morphologies include tripod, v-shape, y-shape, "merge-y", and "higher-order" structures. Preliminary optical studies of both straight and branched NWs are reported, including estimates of the absorption cross section and electrochemical band offsets. Such NWs open up avenues for further investigating the effects of size and shape on the optical/electrical properties of 1D nanomaterials and also have potential uses as active elements in photovoltaics and/or polarization sensitive photodetectors.

## Introduction

Among practical alternatives to crystalline silicon, CdTe is an attractive material for potential low cost photovoltaics.[1] Its near-infrared band gap ($E_g \sim 1.5$ eV, 827 nm, 300 K)[2] and large bulk absorption coefficient ($>10^4$ cm$^{-1}$ in the red, approaching $10^5$ cm$^{-1}$ in the blue)[3] make it an ideal material for matching photovoltaic responses to the visible part of the solar spectrum. Resulting thin film CdTe solar cells have demonstrated external efficiencies meeting or exceeding 16%.[4] In addition to these attractive qualities, many ways for making such films exist.[1] The use of molecular precursors for creating extended CdTe solids is notable. First described by Steigerwald,[5] direct extensions of this work have focused on the development of low dimensional (nanoscale) CdTe. While the primary goal of these studies has been the synthesis of colloidal CdTe quantum dots [QDs, alternatively nanocrystals (NCs)],[6−14] interest in analogous one-dimensional (1D) CdTe nanowires abound.[15−19]

CdTe is an interesting material for other reasons. In addition to properties that make it suitable for photovoltaics,[20] light emitting diodes,[21,22] biological sensors,[23,24] and possibly nanoscale electronics,[25] CdTe, like many other materials,

* To whom correspondence should be addressed. E-mail: mkuno@nd.edu.
† Department of Chemistry and Biochemistry and Notre Dame Radiation Laboratory
‡ University of Waterloo.
§ Department of Electrical Engineering, University of Notre Dame.

(1) Mathew, X.; Thompson, G. W.; Singh, V. P.; McClure, J. C.; Velumani, S.; Mathews, N. R.; Sebastian, P. *J. Sol. Mater.* **2003**, *76*, 293.
(2) Landolt Bornstein, Group III, Springer-Verlag: 1961.
(3) Mitchell, K.; Fahrenbruch, A. L.; Bube, R. H. *J. Appl. Phys.* **1977**, *48*, 829.
(4) Wu, X. *Sol. Energy* **2004**, *77*, 803.
(5) Brennan, J. G.; Siegrist, T.; Carroll, P. J.; Stuczynski, S. M.; Reynders, P.; Brus, L. E.; Steigerwald, M. L. *Chem. Mater.* **1990**, *2*, 403. Steigerwald, M. L.; Sprinkle, C. R. *J. Am. Chem. Soc.* **1987**, *109*, 7200. Kisker, D. W.; Steigerwald, M. L.; Kometani, T. Y.; Jeffers, K. S. *Appl. Phys. Lett.* **1987**, *50*, 1681.
(6) Didenko, Y. T.; Suslick, K. S. *J. Am. Chem. Soc.* **2005**, *127*, 12196.
(7) Yang, Y. A.; Wu, H.; Williams, K. R.; Cao, Y. C. *Angew. Chem., Int. Ed.* **2005**, *44*, 6712.
(8) Zhang, H.; Wang, L.; Xiong, H.; Hu, L.; Yang, B.; Li, W. *Adv. Mater.* **2003**, *15*, 1712.
(9) Wuister, S. F.; van Driel, F.; Meijerink, A. *Phys. Chem. Chem. Phys.* **2003**, *5*, 1253.
(10) Gaponik, N.; Talapin, D. V.; Rogach, A. L.; Hoppe, K.; Shevchenko, E. V.; Kornowski, A.; Eychmuller, A.; Weller, H. *J. Phys. Chem. B* **2002**, *106*, 7177. Talapin, D. V.; Haubold, S.; Rogach, A. L.; Kornowski, A.; Haase, M.; Weller, H. *J. Phys. Chem. B* **2001**, *105*, 2260. Gao, M.; Kirstein, S.; Mohwald, H.; Rogach, A. L.; Kornowski, A.; Eychmuller, A.; Weller, H. *J. Phys. Chem. B* **1998**, *102*, 8360.
(11) Peng, Z. A.; Peng, X. G. *J. Am. Chem. Soc.* **2001**, *123*, 183.
(12) Rajh, T.; Micic, O. I.; Nozik, A. J. *J. Phys. Chem.* **1993**, *97*, 11999.
(13) Jose, R.; Biju, V.; Yamaoka, Y.; Nagase, T.; Makita, Y.; Shinohara, Y.; Baba, Y.; Ishikawa, M. *Appl. Phys. A* **2004**, *79*, 1833.
(14) Mikulec, F. V.; Bawendi, M. G. *Mater. Res. Soc. Symp. Proc.* **2000**, *581*, 139.
(15) Kumar, S.; Ade, M.; Nann, T. *Chem. Eur. J.* **2005**, *11*, 2220.
(16) Tang, Z.; Kotov, N. A.; Giersig, M. *Science* **2002**, *297*, 237.
(17) Volkov, Y.; Mitchell, S.; Gaponik, N.; Rakovich, Y.; Donegan, J. F.; Kelleher, D.; Rogach, A. L. *ChemPhysChem.* **2004**, *5*, 1600.
(18) Ohgai, T.; Gravier, L.; Hoffer, X.; Ansermet, J. P. *J. Appl. Electrochem.* **2005**, *35*, 479.
(19) Zhao, A. W.; Meng, G. W.; Zhang, L. D.; Gao, T.; Sun, S. H.; Pang, Y. T. *Appl. Phys. A* **2003**, *76*, 537.
(20) Kumar, S.; Nann, T. *J. Mater. Res.* **2004**, *19*, 1990.
(21) Gaponik, N. P.; Talapin, D. V.; Rogach, A. L.; Eychmuller, A. J. *Mater. Chem.* **2000**, *10*, 2163. Gaponik, N. P.; Talapin, D. V.; Rogach, A. L. *Phys. Chem. Chem. Phys.* **1999**, *1*, 1787.
(22) Gao, M.; Lesser, C.; Kirstein, S.; Mohwald, H.; Rogach, A. L.; Weller, H. *J. Appl. Phys.* **2000**, *87*, 2297.

10.1021/cm061559m CCC: $33.50 
Published on Web 11/07/2006

exhibits phase admixtures. These mixtures exist because both CdTe's cubic zincblende (ZB) and hexagonal wurtzite (W) phases have similar energies. Predicted energy differences are 9 meV/2 atom.[26] Consequently, it has been possible to exploit polytypism in CdTe to achieve shape control over quasi-0D nanostructures.[27−31] This has led to the subsequent development of colloidal tetrapods as well as other morphologies, not only in CdTe but also in CdSe.[32] In all cases, motivating these shape control studies is the understanding that the optical and electrical properties of nanoscale materials are both size- and shape-dependent.[33]

The current investigation explores many aspects of CdTe, although the primary focus is the synthetic development of both straight and branched CdTe nanowires. Toward this end, we have actively leveraged recent advances in the synthesis of branched (quasi-0D) nanostructures with incipient approaches for creating solution-based 1D NWs.[34−38] Specifically, low melting bimetallic "catalyst" particles are employed to induce directed 1D wire growth within solutions containing common metal and chalcogen precursors. Their selection, as well as the choices of complementary metal binding ligands, coordinating solvents, and growth conditions, all borrow from existing syntheses of colloidal CdTe QDs. Resulting (straight) CdTe NWs have narrow diameters, lengths exceeding 10 $\mu$m in many cases, and diameter size distributions on the order of 15%. Phase-induced NW branching is studied to examine the effects of growth conditions on morphology. Resulting branched CdTe NWs exhibit tripod, v-shape, y-shape, "merge-y", and "higher-order" structures. Their growth directions, diameters, and lengths are all analogous to those of their straight counterparts. Preliminary optical studies of both types of NWs, including absorption cross sections and band offsets, are also reported. Such straight and branched CdTe nanowires may have potential uses in photovoltaics and polarization sensitive photodetectors.[39]

## Experimental Section

**Materials.** The following chemicals were purchased and used as received unless otherwise noted. Chloroform, methanol, hexanes, and toluene were purchased from Fisher Scientific. Dimethylcadmium ($CdMe_2$) was purchased from Strem, passed through a 0.2 $\mu$m PTFE syringe filter in a glovebox, and stored at low temperatures. The usual precautions about working with short chain metal alkyls apply. Specifically, $CdMe_2$ is pyrophoric and moisture sensitive, and can be absorbed through the skin. Employed phosphine-based reagents include: trioctylphosphine oxide (TOPO, 99%, Aldrich), trioctylphosphine (TOP, 90%, Aldrich), and tributylphosphine (TBP, 95%, Aldrich). Phosphonic acids utilized include hexylphosphonic acid (HPA, Alfa Aesar), decylphosphonic acid (DPA, 98%, Lancaster), tetradecylphosphonic acid (TDPA, 97%, Alfa Aesar), and octadecylphosphonic acid (ODPA, 93%, Alfa Aesar). Te shot (200 mesh, 99.8%) was purchased from Aldrich whereas dodecylamine (DDA, 98%) was purchased from Acros.

Tributylphosphine telluride (TBP-Te,∼ 0.5M) was made by mixing 0.32 g (2.5 mmol) Te shot with 5 mL TBP in a glovebox. The solution was allowed to stir overnight, enabling the chalcogen complex to form. The resulting precursor was then filtered through a 0.2 $\mu$m PTFE filter to remove any undissolved material, yielding a clear yellow solution. An analogous procedure was used to make TOP-Se of various molarities.

Bimetallic Au/Bi nanoparticles (NPs) were made as described in the literature.[36] Briefly, the procedure entails making 1.5 nm diameter Au NPs through the biphasic reduction of Au. Resulting particle diameters are 1.5 nm with an ∼18% (as made) size distribution. The Au NPs are then coated with Bi using standard "overcoating" approaches. Reaction temperatures range from 100 to 150 °C, and a mixture of phenyl ether and TOP is used as a coordinating solvent. More specifically, many of the CdTe preparations described herein are conducted using "small" (∼1.4−1.5 nm diameter) Au/Bi NPs. They are prepared by adding 30 $\mu$L (0.184 mmol) of triethylbismuth ($BiEt_3$) to a quarter of the initial Au NP stock.[36] Once coated, the particles are precipitated from solution using acetonitrile. The Au/Bi catalyst is then redissolved in toluene along with a few drops of oleic acid to preserve its stability.[36] The concentration of the solution is subsequently adjusted to yield an absorbance of 0.126 at 500 nm (∼0.38 mM),[36] allowing one to "calibrate" the mixture. This ensures more reproducible NW syntheses and allows a comparison to previous studies. The resulting Au/Bi solution is stored in a glovebox freezer and keeps for several months with no adverse effects on the synthesis.

**Synthesis of Straight NWs.** A typical preparation of straight CdTe NWs proceeds as follows. TOPO (99%, 10 g, 0.028 mol), TOP (90%, 11.5 mL, 0.026 mol), TBP-Te (0.5 M, 0.05 mL, 25 $\mu$mol Te), and DPA (0.071 g, 0.32 mmol) are added to a 100 mL three neck flask. Alternatively, other phosphonic acids can be used in place of DPA. For example, HPA (0.053 g, 0.32 mmol), TDPA (0.089 g, 0.32 mol), and ODPA (0.10 g, 0.32 mmol) all yield similar quality (straight) NWs. Once the reagents have been added, the apparatus is connected to a Schlenk line. Its contents are heated under vacuum at ∼130−150 °C to dry and degas the mixture. The three neck flask is then backfilled with $N_2$ and is heated to 275 °C.

In a glovebox, an injection solution consisting of 175 $\mu$L (∼0.067 $\mu$mol) of the Au/Bi stock and 11 $\mu$L $CdMe_2$ (∼0.16 mmol) is prepared. The resulting metal to chalcogen (metal to phosphonic

(23) Wang, S.; Mamedova, N.; Kotov, N. A.; Chen, W.; Studer, J. *Nano Lett.* **2002**, *2*, 817.
(24) Mamedova, N. N.; Kotov, N. A.; Rogach, A. L.; Studer, J. *Nano Lett.* **2001**, *1*, 281.
(25) Wang, Y.; Tang, Z.; Tan, S.; Kotov, N. A. *Nano Lett.* **2005**, *5*, 243.
(26) Wei, S-H.; Zhang, S. B. *Phys. Rev. B* **2000**, *62*, 6944.
(27) Manna, L.; Milliron, D. J.; Meisel, A.; Scher, E. C.; Alivisatos, A. P. *Nat. Mater.* **2003**, *2*, 382.
(28) Kanaras, A. G.; Sonnichsen, C.; Liu, H.; Alivisatos, A. P. *Nano Lett.* **2005**, *5*, 2164.
(29) Yu, W. W.; Wang, A.; Peng, X. *Chem. Mater.* **2003**, *15*, 4300.
(30) Bunge, S. D.; Krueger, K. M.; Boyle, T. J.; Rodriguez, M. A.; Headley, T. J.; Colvin, V. L. *J. Mater. Chem.* **2003**, *13*, 1705.
(31) Shieh, F.; Saunders, A. E.; Korgel, B. A. *J. Phys. Chem. B* **2005**, *109*, 8538.
(32) Manna, L.; Scher, E. C.; Alivisatos, A. P. *J. Am. Chem. Soc.* **2000**, *122*, 12700.
(33) Gaponenko, S. V. *Optical Properties of semiconductor nanocrystals*; Cambridge University Press: New York, 1988.
(34) Trentler, T. J.; Hickman, K. M.; Goel, S. C.; Viano, A. M.; Gibbons, P. C.; Buhro, W. E. *Science* **1995**, *270*, 1791. Yu, H.; Buhro, W. E. *Adv. Mater.* **2003**, 15, 416. Yu, H.; Li, J. B.; Loomis, R. A.; Wang, L. W.; Buhro, W. E. *Nat. Mater.* **2003**, *2*, 517. Yu, H.; Loomis, R. A.; Gibbons, P. C.; Wang, L-W.; Buhro, W. E. *J. Am. Chem. Soc.* **2003**, *125*, 16168.
(35) Holmes, J. D.; Johnston, K. P.; Doty, R. C.; Korgel, B. A. *Science* **2000**, *287*, 1471. Davidson, F. M.; Schricker, A. D.; Wiacek, R. J.; Korgel, B. A. *Adv. Mater.* **2004**, *16*, 646.
(36) Grebinksi, J. W.; Richter, K. L.; Zhang, J.; Kosel, T. H.; Kuno, M. *J. Phys. Chem. B* **2004**, *108*, 9745.
(37) Grebinski, J. W.; Hull, K. L.; Zhang, J.; Kosel, T. H.; Kuno, M. *Chem. Mater.* **2004**, *16*, 5260.
(38) Hull, K. L.; Grebinski, J. W.; Kosel, T. H.; Kuno, M. *Chem. Mater.* **2005**, *17*, 4416.
(39) Singh, A.; Li, X.; Jena, D.; Xing, H.; Protasenko, V.; Kuno, M. In preparation.

acid) mole ratio is 6:1 (at least 2:1). The Au/Bi NP/$CdMe_2$ solution is then mixed and loaded into a 1 mL disposable syringe. When the temperature of the Te solution reaches 275 °C, the injection solution is brought out of the glovebox and is introduced into the mixture to initiate the reaction. On injection, the solution's color rapidly turns dark brown/black. The reaction is then allowed to sit at temperature for 1 min before the heating mantle is removed. Generally, no precipitation occurs after the injection, but on occasion, a flocculate is observed. Resulting diameters, size distributions, and lengths, however, do not differ noticeably from those measured in other NW preparations where the precipitation event is absent.

After the synthesis, the NWs are processed as follows. Toluene (~10 mL) is added to the flask to prevent TOPO from solidifying. An excess of methanol is then introduced to precipitate the NWs. Alternatively, other polar solvents such as ethanol or isopropanol can be added to achieve the same effect. The suspension is then centrifuged at 4400 rpm whereupon the resulting supernatant is discarded. The recovered precipitate is then resuspended in hexanes, shaken, briefly sonicated and centrifuged once more. Again, the resulting supernatant is discarded, and hexanes are added to the precipitate. The recovered material is then "washed" several more times. Repeated exposure to hexanes dramatically reduces the amount of excess surfactant present in solution. Once cleaned, the NWs can be resuspended in either toluene or chloroform. A small amount of either DDA or tetraoctylammonium bromide (TOAB) can be added to help maintain the solubility of the NWs.

**Synthesis of Branched NWs.** The synthesis of branched CdTe NWs proceeds in the same manner. Briefly, the same mixture of TOPO, TOP, TBP-Te, and DPA (or other phosphonic acids) is added to the flask and is dried/degassed. An injection solution, identical to that used for making straight NWs, is also prepared. On injection, the mixture is allowed to remain at temperature for 1 min before the heating mantle is removed. Identical methods are then used to precipitate, resuspend, and wash the NWs. Notable differences, however, include a higher injection temperature ($T \geq$ 285 °C), and occasionally a different (less stoichiometric) Cd:Te precursor mole ratio.

**Control Experiments.** To test the compatibility of various Te precursors with the Au/Bi catalyst, small amounts of each were mixed and allowed to react. These control experiments revealed that direct exposure of the catalyst to commonly available Te precursors resulted in a black precipitate (likely $Bi_2Te_3$). Common Te precursors investigated include TOP-Te,[40] TBP-Te,[40] HPPTTe,[14] and $TeCl_4$.[41,42] When needed, the above Te precursors were prepared following literature procedures. The molarity of the Te solution was also varied to see the effects of concentration on the precursor/Au/Bi NP reactivity. In general, more Te basic compounds such as HPPTTe, and more dilute conditions, retarded the onset of precipitation. However, given the overall instability of the mixture, it was concluded that common Te precursors should not be directly exposed to the bimetallic catalyst. By contrast, $CdMe_2$ and the Au/Bi catalyst were found to be compatible. This led to modifications of our general approach for making solution-based NWs.[36−38] The resulting variation, described above, is akin to more traditional "organometallic" preparations for colloidal QDs.[40]

The need for a Au/Bi catalyst was also tested. Specifically, the Au/Bi NP solution was replaced with 175 $\mu$L of toluene, and reactions were conducted in the manner described above. In all cases, the resulting product consisted of highly fluorescent CdTe QDs with no sign of NWs.

**Instrumentation.** Samples for low- and high-resolution transmission electron microscopy (TEM) were prepared by dropping a dilute toluene or chloroform solution of NWs onto ultrathin carbon coated grids (Ladd). Survey TEMs were conducted using a JEOL 100SX transmission electron microscope. High-resolution images were obtained with a JEOL 2010 microscope operating at 200 kV. Both low- and high-resolution TEM micrographs were taken using the latter instrument. Elemental analysis was conducted using an energy dispersive X-ray spectroscopy (EDXS) analyzer attached to the 2010. A Cliff−Lorimer algorithm was employed for the standardless quantification of sample compositions. UV−vis absorption spectra were acquired with a Cary 50-Bio UV−vis spectrophotometer. A Perkin-Elmer Optima 3300XL ICPAES unit was used to quantify the elemental concentration of various test samples. Commercial Cd, Se, and Te atomic emission standards were purchased from Fisher Scientific to quantify the results. Electrochemical measurements were conducted through cyclic voltammetry, using a conventional three electrode cell. Acetonitrile and tetrabutylammonium perchlorate were used as a solvent and electrolyte, respectively. Ultrafast transient differential absorption spectra were acquired with a Clark MXR CPA 2010 laser system coupled to an Ultrafast Systems pump−probe detection scheme. The 387 nm (3.2 eV) second harmonic of the laser fundamental was used to excite samples while a white light probe (420−800 nm, 1.5−2.9 eV) was generated by passing a fraction of the fundamental through a sapphire plate. A delay line provided probe delays ranging from 150 fs to 1.5 ns. X-ray diffraction spectra were acquired with Cu K$\alpha$ ($\lambda$ = 1.54 Å) radiation using a Bruker D8 Advance diffractometer. Samples were prepared by first dropping concentrated suspensions of NWs in toluene or cholorform onto a 6° offcut single (0001) crystal quartz plate.

## Results and Discussion

**Synthesis.** The current CdTe preparation is a variation of an existing solution-phase synthesis for confined CdSe NWs.[34,36,37] Low melting bimetallic "catalyst" NPs are used to induce nanowire growth within reaction mixtures containing common metal and chalcogen precursors. The bimetallic catalyst consists of a Au core and a Bi shell.[36] Use of Au NPs as templates for the core/shell species is motivated by their facile synthesis and narrow diameters (~1.5 nm). The selection of Bi is guided by its low bulk melting point (~271 °C) and, more importantly, by its successful use in promoting the growth of both CdSe and PbSe NWs.[34,36,37]

Although the actual detailed growth mechanism involving the Au/Bi NPs is not known, it is thought to mimic the vapor−liquid−solid (VLS) growth of both nanowires[43] and semiconductor whiskers.[43,44] Essentially, Cd and Te in the solution originate from the thermolysis of $CdMe_2$ and TBP-Te. The elements subsequently dissolve into the Au/Bi NPs, the surface of which serves as a heterogeneous nucleation site for CdTe. Passivation of the resulting CdTe NW surface by TOP and TOPO prevents further growth onto the CdTe/solution interface whereupon continued NW growth occurs by diffusion of Cd and Te through the NP to the growing end of the wire. Indirect evidence for this seeded growth mechanism can be seen in cases where the NP is observed

(40) Murray C. B.; Norris, D. J.; Bawendi, M. G. *J. Am. Chem. Soc.* **1993**, *115*, 8706.
(41) Yu, H.; Gibbons, P. C.; Buhro, W. E. *J. Mater. Chem.* **2004**, *14*, 595.
(42) Cordes, A. W.; Kruth, R. F.; Gordon, E. K.; Kemp, M. K. *Acta Crystallogr.* **1964**, *17*, 756.
(43) Wagner, R. S.; Ellis, W. C. *Appl. Phys. Lett.* **1964**, *4*, 89.
(44) Givargizov, E. I. *J. Cryst. Growth* **1975**, *31*, 20.

still attached to the end of a NW. This has previously been seen in CdSe[37] as well as in the current study (Supporting Information, Figure 3). Further evidence for a seeded growth mechanism includes the lack of NW formation in the absence of catalyst particles (see the Experimental Section, Control Experiments subsection) and blunt NW ends, indicating where a catalyst particle once resided.[37]

The above reaction is conducted in the presence of a mild coordinating solvent, a 1:1 mixture of TOP and TOPO. Use of TOPO borrows from existing syntheses for CdSe and CdTe QDs where it is often employed as a high boiling coordinating solvent.[11,40] Given the small (uncontrolled) amounts of phosphonic and/or phosphinic acids in technical grade (90%) TOPO, high purity material (99%) is utilized in all cases to suppress any reproducibility issues.[40,45] Similarly, the use of TOP is motivated by studies showing it to be a good passivating agent, leading to the development of highly fluorescent CdTe QDs.[10] In the current synthesis, the 1:1 TOP/TOPO mixture was found to be ideal for growing high quality CdTe NWs. Other solvents/solvent mixtures such as TOPO and TOP alone as well as phenyl ether, octyl ether, and primary amines such as DDA were evaluated. None yielded CdTe NWs of the same quality as the 1:1 TOP/TOPO mixture.

Both TOP and TOPO bind datively to the NW surface, providing electronic passivation of dangling bonds and suppressing surface oxidation. This is relevant since analogous CdTe QDs are known to be somewhat air sensitive.[14] The resulting, surface passivated, CdTe NWs are soluble in common organic solvents such as toluene or chloroform. As such, additional surface functionalization chemistries are possible to make the wires water soluble and/or biocompatible. These features distinguish solution-based NWs from VLS grown samples. Additional features/advantages over VLS preparations include their low cost, potential scalability, and moderate growth temperatures, often below 300 °C.

Figure 1a shows low-resolution TEM micrographs of straight CdTe NW ensembles. The wires are flexible and in many cases have lengths which exceed 10 $\mu$m. Diameters range from 8 to 10 nm and are below twice the bulk exciton Bohr radius of the material ($a_B = 7.5$ nm).[46] Size distributions of as made ensembles have been estimated by measuring the diameters of more than 250 wires. Resulting values range from 14% to 20% and are, on average, narrower than the distributions found within comparable CdSe NWs (~20−30%).[37] Furthermore, intrawire diameter distributions, obtained by measuring 6−7 spots on a given wire for the same 250 wires, were found to be on the order of 5% ($\sigma = 2\%$). This illustrates the uniformity of the wires and is again comparable to intrawire diameter distributions seen in analogous CdSe NWs. Low-resolution micrographs of branched CdTe NWs are provided in Figure 1b, and the general morphology of such branched wires will be discussed shortly. Additional low-resolution TEM images of both straight and branched NWs can be found in the Supporting Information.

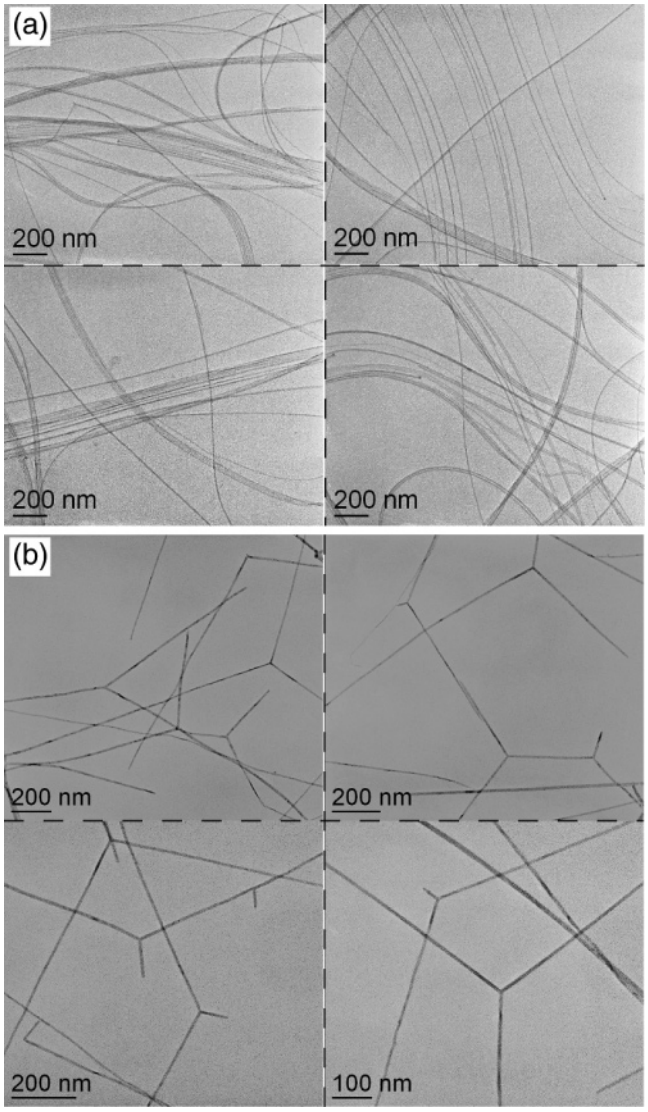


**Figure 1.** Low-resolution TEM micrographs of (a) straight and (b) branched CdTe NWs.

High-resolution TEM (HRTEM) micrographs of straight NWs are shown in Figure 2a,b. Figure 2a illustrates narrow diameter (5−6 nm) CdTe NWs. Three adjacent wires from a different ensemble, with corresponding widths ranging from 8 to 10 nm, are shown in Figure 2b. Additional high-resolution micrographs are provided in the Supporting Information.

ZB/W phase admixtures, as well as twinning within ZB sections, are observed in both CdSe and CdTe NWs. All NWs grow along the <111> and <0001> directions of the CdTe zincblende (ZB) and wurtzite (W) phases, as determined through HRTEM images. This parallels the behavior of solution-grown CdSe NWs.[37] To illustrate, Figure 3 shows HRTEM images of CdTe NWs viewed along a <110> zone, normal to the <111>/<0001> growth axis. Sections of ZB and W as well as twinning are evident through "zigzag" patterns in the lattice images.[37] These fringes can only be observed within properly oriented wires or in those samples that have been deliberately tilted in the TEM. This happens because a simple rotation of the NW to a more common non-<110> zone (Figure 2b, for example) reveals only parallel lattice fringes, obscuring the phase admixture/

(45) Kuno, M.; Higginson, K. A.; Qadri, S. B.; Yousuf, M.; Lee, S-H.; Davis, B. L.; Mattoussi, H. *J. Phys. Chem.* **2003**, *107*, 5758.
(46) Yoffe, A. D. *Adv. Phys.* **2002**, *51*, 799.

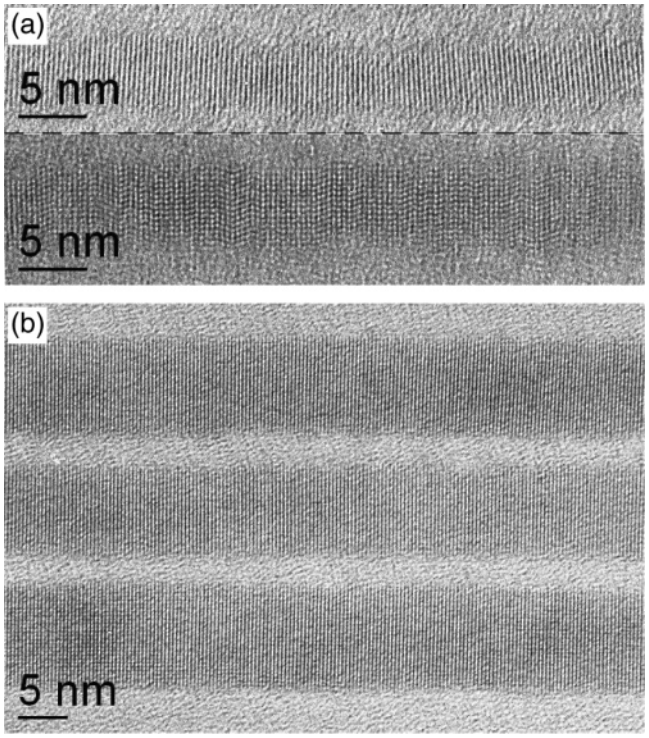


**Figure 2.** High-resolution TEM images of (a) narrow (5−6 nm) and (b) thicker (8−10 nm) straight CdTe NWs.

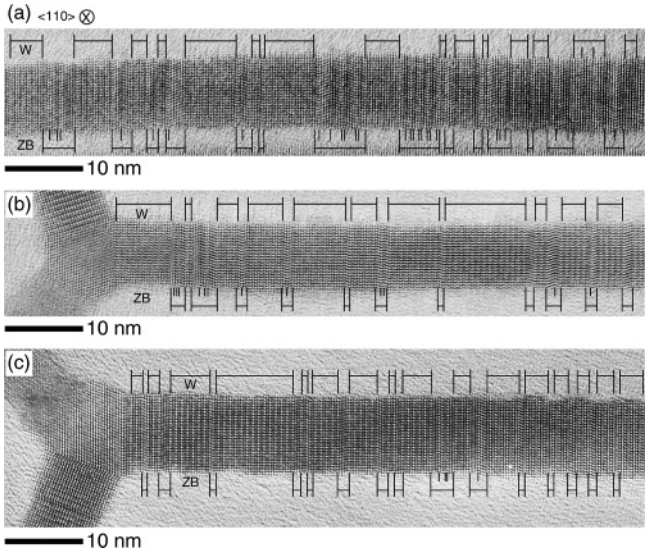


**Figure 3.** High-resolution TEM micrographs illustrating the ZB/W phase admixture in (a) straight and (b, c) branched CdTe NWs. In all cases, the observation direction is <110> normal to the <111>/<0001> NW growth axis.

twinning present in the wires.[37] We find that the average ZB length in CdTe NWs is 2 nm ($\sigma = 4$), while the average W length is 3 nm ($\sigma = 7$). These lengths are statistically identical to values measured in complementary CdSe NWs.[37]

The presence of both ZB and W likely stems from the low energy difference between the two phases. In particular, a 9 meV/2 atom energy difference exists in CdTe.[26] Likewise, a smaller 2 meV/2 atom energy difference exists in CdSe.[26] As a consequence, it is not difficult to envision how this phase change occurs during growth. Specifically, along the <111>/<0001> growth direction, a transition from ZB to W simply entails a 60° rotation of the bond from a staggered to an eclipsed configuration between {111}/{0001} planes.[37] Furthermore, since no periodicity is observed in the phase admixture, random fluctuations in the reaction conditions (possibly temperature related) could induce these transitions during growth.

Apart from phase admixtures/twinning, common to this and earlier solution-based NW preparations is the use of ligand-coordinated metal precursors. Specifically, coordinating $Cd^{2+}$ with phosphonic and/or fatty acids introduces additional control over the NW growth kinetics. This occurs because their tunable stability constants (*K*'s) help dictate the concentration of reactive metal ions in solution during the reaction.[45] The selection of an appropriate metal-coordinating ligand is ultimately determined through trial and error. In this respect, phosphonic acids were found to be optimal for growing CdTe NWs whereas fatty acids were found to be suitable for producing high quality CdSe and PbSe NWs.[36−38]

One difference between the current synthesis and previous NW preparations is the use of dimethylcadmium (as opposed to CdO) and its injection into reaction mixtures containing chalcogen precursors (i.e., TOP-Te). By contrast, previous preparations of CdSe[36,37] and PbSe[38] NWs have entailed injecting mixtures of TOP-Se and Au/Bi NPs into solutions containing ligand-coordinated metal ions. The motivation for the reversal is the incompatibility of common tellurium precursors (TOP-Te, TBP-Te, HPPTTe, and $TeCl_4$) with the Au/Bi catalyst (Experimental Section). Specifically, on mixing the two, a reaction occurs, giving a black precipitate thought to be $Bi_2Te_3$. Nanowires subsequently prepared using these solutions have low yields, poor size distributions, and a low overall quality. The choice of $CdMe_2$ as an alternative metal source is motivated by its successful use in previous colloidal CdSe and CdTe QD syntheses.[40] Furthermore, it has been found to be compatible with the Au/Bi catalyst (Experimental Section).

Other comparisons to previous NW preparations are noted. For example, the concentration of the reaction mixture (i.e., the amount of Au/Bi NPs, Cd and Te precursor for a given amount of TOP/TOPO) is an important parameter, which dictates the quality of the resulting NWs.[37] Both current and previous NW preparations have shown that, on injection, a concentrated TOP/TOPO mixture preferentially yields QDs rather than NWs. This illustrates the underlying competition between catalyzed NW growth and uncatalyzed QD growth. By contrast, very dilute reaction mixtures promote the uncatalyzed "transverse" growth of NW diameters over their lengths. As a consequence, resulting NWs are noticeably thicker than counterpart wires made under more concentrated conditions. An optimal reaction mixture concentration is therefore found empirically.

The amount of catalyst used in the injection solution also dictates the quality of the resulting NWs.[37] Specifically, too little catalyst favors QD over NW growth. Conversely, too much leads to noticeable Au/Bi aggregates, reducing the overall quality of the ensemble. This is especially problematic with PbSe.[38] Again, an optimal amount of catalyst, yielding high quality CdTe NWs, is found empirically (100−175 $\mu$L, 36−67 nmol).

Finally, although the NW diameter is ultimately influenced by a number of factors, it is primarily determined by the catalyst size. Specifically, small Au/Bi NPs (~1.4−1.5 nm) yield narrow diameter NWs, whereas larger particles (>2 nm) yield thicker wires. As such, an approximate proportionality exists between the NW diameter and that of the catalyst. This matches general trends seen in the seeded (VLS) growth of nanowires.[47] In practice, NW diameters are often much larger than their corresponding catalyst. For example, in the current CdTe synthesis, the NP size most commonly employed is 1.4−1.5 nm. The diameter of the resulting NWs, by contrast, typically ranges from 5 to 10 nm. This discrepancy may arise from "swelling" of the Au/Bi NP with metal/chalcogen atoms prior to supersaturation and is supported by TEM images of catalyst particles attached to NW ends (Supporting Information).[37] As such, an induction period likely exists prior to NW growth during which alloying of the catalyst occurs.

One of the more notable parameters in the synthesis of straight NWs is the metal to chalcogen ratio. In general, straight CdTe NW preparations appear optimal when the reaction mixture is Cd rich. For example, in the current synthesis, a 6:1 Cd:Te mole ratio is used make straight NWs. A similar behavior is observed in CdSe and PbSe NWs.[37,38] In the former case, the employed Cd:Se mole ratio is 7:1[37] whereas in the latter case, a 2:1 Pb:Se mole ratio is preferred.[38] Although the exact reason for this asymmetry, leading to straight NWs, is not known, we speculate that it may relate to differing metal/chalcogen solubilities within the Bi shell.[37] In all cases, ICPAES elemental analyses of the resulting NWs show average Cd to Te atom fractions of 49% ($\sigma$ = 2%) and 51% ($\sigma$ = 2%), respectively. A representative EDXS spectrum is also provided in the Supporting Information.

Changing the metal/chalcogen mole ratio to more stoichiometric values (1.7:1) yields branched CdSe NWs.[37] The same is true with CdTe, for which decreasing the metal/chalcogen ratio into the range between 2:1 and 1:6 increases branching. However, this approach to branching is not used in practice since the resulting wires are poor in quality. An opposite trend is observed with PbSe where a more asymmetric 4:1 metal/chalcogen mole ratio is preferred.[38] Again, these varied responses and overall branching sensitivity to the metal/chalcogen mole ratio may arise from differing metal/chalcogen solubilities within the catalyst. Furthermore, differences in the local concentration of metal/chalcogen atoms in solution may influence the nucleation rate of the resulting semiconductor. This can, in turn, lead to situations where multiple NWs grow out of a given NP, leading to branched NWs. Such a scenario, called a "geminate" nanowire nucleation mechanism, has been discussed in more detail in ref 37.

Figure 4a−d shows high-resolution TEM images of CdTe tripods. These wires are analogous to counterpart CdSe NWs having the same shape. In this respect, the branching point of both CdTe and CdSe NWs is a triangular ZB section with four equivalent {111} faces. A cartoon illustrating this is provided in the Supporting Information. From these faces, additional "arms" arise, resulting in branched CdTe NWs. Specifically, tripod (Figure 4a−d), v-shape (Figure 5a−d), and y-shape (Figure 6a−d) NWs are all characterized by a central triangular ZB core with 3, 2, and 3 arms extending from it, respectively. Each arm grows along the <111>/<0001> directions of the ZB/W phase of CdTe much like straight NWs. All arms, labeled α, $\beta$, $\gamma$ (α′), exhibit ZB/W phase admixtures as well as twinning. Within tripods, no evidence of a fourth arm is found, on the basis of field emission SEM measurements.[37] Furthermore, the merge-y structure (Figure 7a−d) is unique in that it consists of two arms conjoined by a grain boundary running down the length of an apparent third arm called $\gamma$. Additional high-resolution

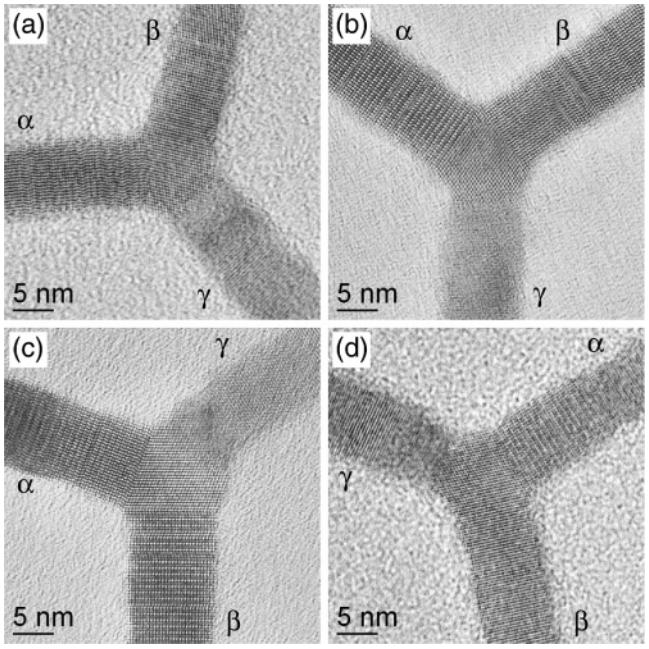


**Figure 4.** (a−d) High-resolution TEM images of tripod shaped CdTe NWs.

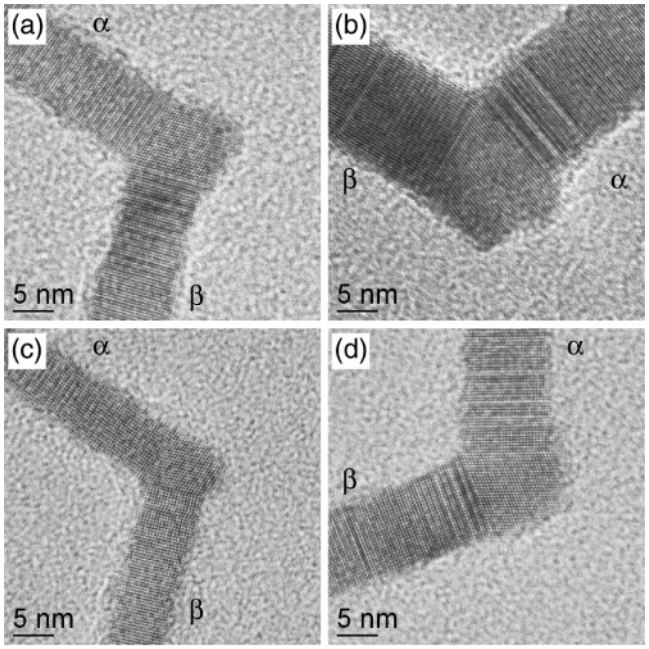


**Figure 5.** (a−d) High-resolution TEM images of v-shaped CdTe NWs.

(47) Wu, Y.; Yan, H.; Huang, M.; Messer, B.; Song, J. H.; Yang, P. *Chem. Eur. J.* **2002**, *8*, 1261.

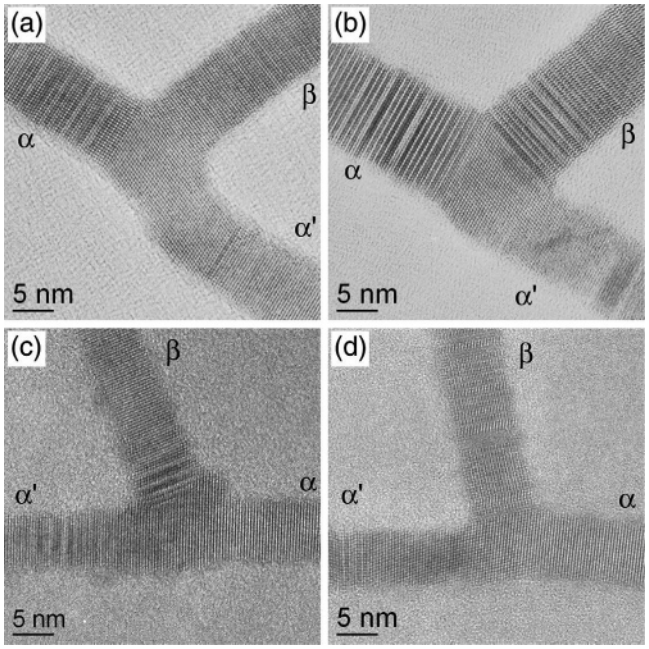


**Figure 6.** (a−d) High-resolution TEM images of y-shaped CdTe NWs.

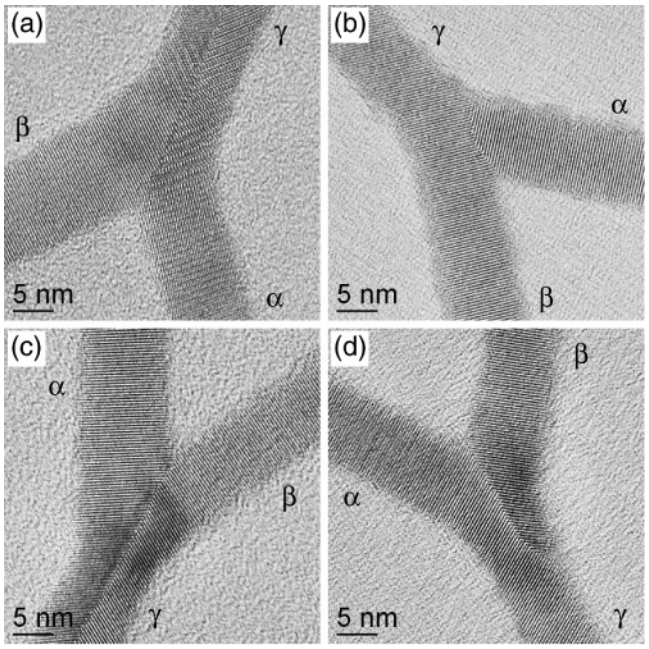


**Figure 7.** (a−d) High-resolution TEM images of merge-y CdTe NWs.

TEM images of branched NWs can be found in the Supporting Information.

Other structural aspects of branched NWs are rationalized by the triangular ZB core. For example, in tripods the average $\alpha\beta$ angle is 106° ($\sigma = 3°$). Complementary $\alpha\gamma$ and $\beta\gamma$ angles are 125° ($\sigma = 4°$) and 129° ($\sigma = 5°$), respectively. The $\alpha\beta$ angle is understood because the angle between two {111} faces is 109.5°. Furthermore, given that α and $\beta$ lie within the plane of the substrate, the much larger $\alpha\gamma$ and $\beta\gamma$ angles are rationalized since the third {111} face and consequently the third arm ($\gamma$) must point out of the substrate by 54.7°.[37] As a result, the apparent $\alpha\gamma$ (or $\beta\gamma$) angle, projected onto the substrate, is 125.3°, in excellent agreement with experimentally observed values. This tilt also explains the difficulty lattice imaging the $\gamma$/ZB core interface.

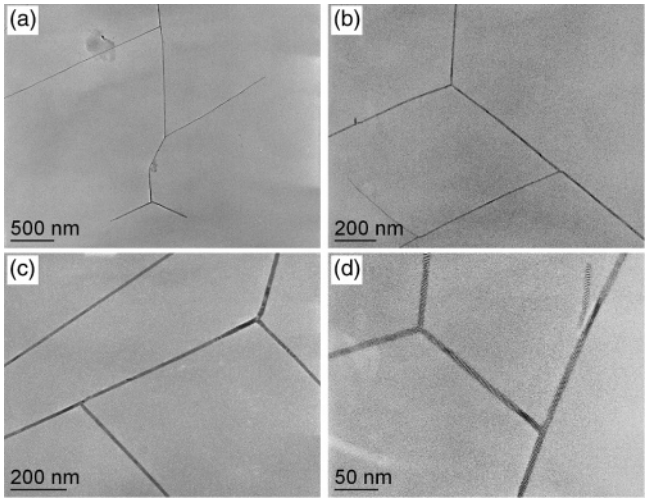


**Figure 8.** (a−d) Low-resolution TEM images of higher order CdTe NWs.

A similar analysis can be conducted with v-shape and y-shape NWs. The average $\alpha\beta$ angle in v-shaped wires is 110° ($\sigma = 1°$) whereas the average $\alpha\beta$ angle in y-shaped wires is 108° ($\sigma = 3°$). Both are consistent with the 109.5° angle expected between equivalent {111} planes. In the latter case, the average $\alpha'\beta$ angle, 73° ($\sigma = 4°$), is rationalized because α′ grows along the same <111> direction as α. As such, the predicted $\alpha'\beta$ angle is 70.5°.

For merge-y NWs the average $\alpha\beta$ angle is 70° ($\sigma = 11°$). This is comparable to that seen with analogous CdSe wires. However, in either case, no unique $\alpha\beta$ or $\alpha\gamma/\beta\gamma$ angles are observed. This is because a high energy, high angle grain boundary runs down the length of the third arm ($\gamma$), and no triangular ZB core exists. By contrast, the $\alpha\beta$ angle in merge-y PbSe is well defined because of a {111} twin plane along $\gamma$.[38] Predicted $\alpha\beta$ angles are 70.5°, in good agreement with an experimentally observed value of 67.3° ($\sigma = 9.6$).

In merge-y NWs, $\gamma$ ultimately reduces its energy by rejecting the grain boundary, whose area decreases as it deviates toward the side of the wire. For example, in Figure 7d rejection of the grain boundary eventually results in $\gamma$ being a crystal of the same orientation as α. This phenomenon is often observed in both CdTe/CdSe merge-y structures with low magnification micrographs showing that, after rejecting the grain boundary, $\gamma$ reverts back to the same <111> growth direction as α or $\beta$.

Extended branching is also observed in CdTe ensembles. To illustrate, Figure 8a−e shows examples of "higher order" ("hyperbranched") structures (additional micrographs in the Supporting Information). These NWs consist of linear combinations of tripod, v-shape, y-shape, and merge-y NWs. Such morphologies have also been seen in branched CdSe as well as PbSe wires.

The mechanism responsible for NW branching has previously been discussed in ref 37. Briefly, this "geminate" NW nucleation mechanism posits that, on achieving suitable conditions, two arms (α, $\beta$) nucleate on a single catalyst particle. A mutual angle ($\theta$) then exists between α and $\beta$. If $\theta$ is less than a critical angle ($\theta_{crit}$, thought to be ∼77°), the two arms quickly touch and accommodate each other through a grain boundary (CdSe and CdTe) or a low energy {111} twin (PbSe).[36−38] This leads to merge-y structures, common

to branched CdSe, CdTe, and PbSe NWs. Conversely, if $\theta$ is larger than $\theta_{crit}$, time exists for the two arms to rotate/reorient on the liquid NP surface, enabling the wires to develop a common ZB (CdSe, CdTe) or rocksalt (PbSe) core. On linking, a branched NW is obtained with tripod, v-shape, and y-shape (CdSe, CdTe) or t-shape and right angle (PbSe) morphologies.[36−38] Other branching mechanisms considered include a catalyst "fission" mechanism and even uncatalyzed NW growth,[37] though none have yielded consistent explanations for NW branching. These alternative mechanisms are described in more detail in ref 37.

In the current synthesis, branching can also be achieved by adding a small amount of Se (i.e., TOP-Se) to the initial Te solution. HRTEM images of these Se-doped NWs are provided in the Supporting Information. ICPAES measurements of the NWs show a 1.5 ($\sigma = 0.7$)% Se incorporation into the wires. In this sense, true ternary $CdSe_xTe_{1-x}$ NWs have not been observed. Specifically, increasing the Se content of the chalcogen solution, under the current conditions (Experimental Section), does not yield branched wires with tunable compositions ($x$). This may be due to the different reactivity of TOP-Te relative to TOP-Se (or solubility of Se vs Te in Bi), enabling the relatively unstable Te compound to dominate the overall growth of the wires. Such behavior may then have implications for the direct substitutional doping of solution-based NWs, since the differing decomposition rates of various precursors must be considered in order to achieve substantial and meaningful dopant incorporation.

The biggest impact in inducing CdTe branching is the temperature at which the synthesis is carried out. Reactions conducted at temperatures below ~275 °C (and in the range between 220 and 275 °C) show no significant branching even when the metal to chalcogen ratio is varied dramatically. Only when the injection/growth temperature exceeds 285 °C does branching occur. This temperature dependence has been seen before. In the case of CdSe, preferential branching at lower temperatures ($T \leq 280$ °C) is observed and is rationalized by suggesting that the nucleation of zincblende (ZB) over wurtzite (W) is favored in this regime.[37] The presence of ZB is relevant since it comprises the center of each branching point in tripod, v-shape, and y-shape NWs. In the case of CdTe, branching at higher temperatures is rationalized by an analogous preference for nucleating ZB at temperatures ≥285 °C. This is supported by studies showing the stability of the CdTe W phase at low temperatures and, conversely, a transition to the ZB phase at higher temperatures.[20] Likewise, theoretical studies suggest the stability of ZB over W in CdSe, rationalizing why branching is favored at low temperatures.[26] In CdTe one might thus predict that NWs made at temperatures below (above) 275 °C (285 °C) have slightly higher concentrations of W (ZB).

In principle, this phase admixture and temperature-dependent ZB/W ratio can be studied by analyzing corresponding X-ray powder patterns. Making such analyses difficult, however, are overlapping ZB/W reflections[20] as well as crystallographic texture.[37] Specifically, when spread on a quartz plate, the NWs will tend to rest with their growth

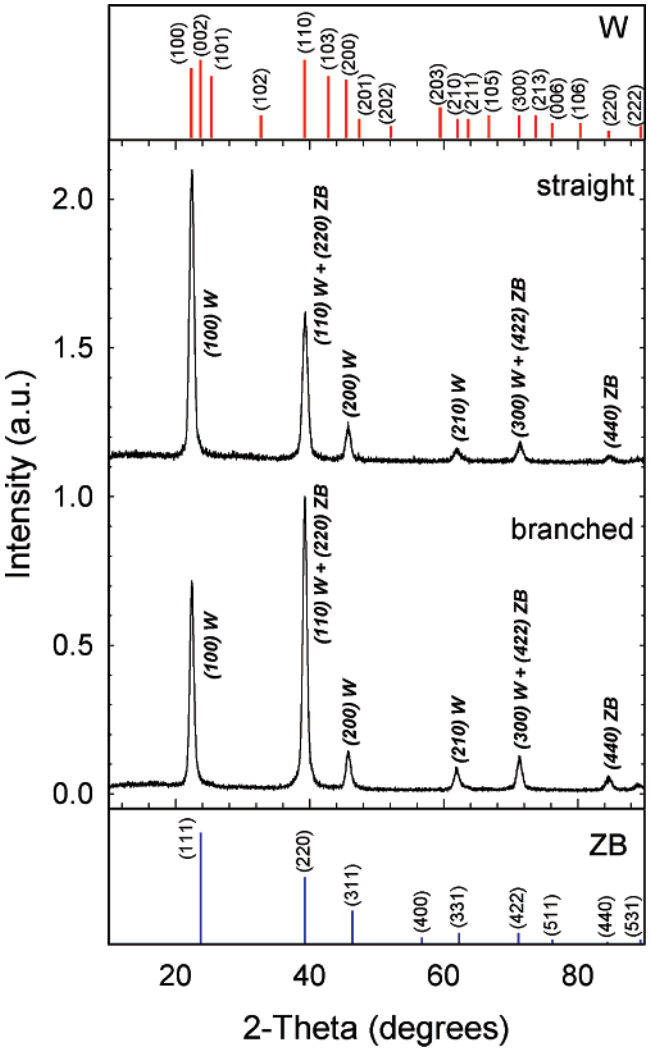


**Figure 9.** X-ray powder patterns of straight and branched CdTe NWs. Stick patterns of bulk ZB and W CdTe are provided for comparison purposes.

axis parallel to the substrate. This has previously been seen with CdSe and PbSe NWs.[37,38] As a consequence, the intensities of various reflections in the experimental powder pattern are distorted relative to the case of randomly oriented grains. Some lines are enhanced while others are suppressed. To illustrate, Figure 9a,b shows powder patterns of straight and branched CdTe NWs. Intensity distortions are readily apparent on comparing the experimental data with the bulk ZB/W JCPDS powder patterns [ZB (JCPDS:15-0770), W (JCPDS:19-0193)] provided in the figure.

The effects of crystallographic texture can be understood because only those planes parallel to the substrate will diffract strongly and be detected by a powder diffractometer. For straight NWs, we assume that to a good approximation all wires lie flat on the surface. As a consequence, in ZB, only planes (*hkl*) parallel to the <111> growth axis are simultaneously parallel to the diffractometer specimen surface. Likewise, in W only planes parallel to the <001> growth axis diffract strongly. ZB segments therefore contribute to the powder pattern only from (220), (422), and (440) planes whereas W segments diffract only from (100), (110), (200), (210), and (300) planes. These predictions are borne out by the absence of many ZB and W reflections in the experi-

mental data. With this understanding, one can interpret one of two dominant lines in the data at 39.3° as originating from an overlap between the (110) W and (220) ZB reflections. The second of these two lines at 22.4° must arise from (100) W only. Additional theoretical assignments are provided in the figure.

In branched NWs, a high probability exists that both α and $\beta$ lie flat on the TEM/diffractometer substrate. This yields examples such as Figures 3−6 in which the triangular ZB core is viewed along a <110> direction, giving a <110> lattice image. As a consequence, both α and $\beta$ have ZB (220) and W (110) parallel to the substrate. This preferred orientation would then add intensity to the 39.3° reflection in addition to any abovementioned ZB/W ratio contributions.

In principle, intensity differences can be modeled through "multiplicity factors" as done previously with PbSe NWs.[38] However, in the current case, without a more accurate estimate of the ZB/W ratio (or NW orientation) in actual samples, theoretical powder patterns cannot be calculated. In all cases, peak broadening is observed and can be attributed to the finite diameters of the NWs, given their high degree of crystallinity (Figures 2−7). Subsequent Scherer analyses also yield diameters consistent with those measured through TEM experiments.

Ultimately, a number of factors play a role in dictating the structure of branched NWs. In this respect, the nucleation of a specific crystal phase is important for the resulting morphology of branched nanostructures. This is true, not only in 1D, but more generally as well.[48,49] Thus, by influencing the nucleation of a given phase one can achieve shape control over the resulting crystal. Complicating phase-induced branching, however, is the role of organic surfactants/metal binding ligands used to control the size and size distribution of the resulting material. While both are used as high boiling solvents, influencing nanostructure growth kinetics, both also impact the phase of the nucleated material. A classic example is the recent discovery of $\epsilon$-cobalt, a cubic phase induced by the presence of TOPO.[50] Numerous examples of this phenomenon now exist in other systems.[48,49] As a consequence, both the kinetic and thermodynamic factors behind nucleation/crystallization must be considered in tandem to achieve true shape control over nanostructures.[48]

**Optical Properties.** The linear absorption of a small size series of CdTe NWs is shown in Figure 10. Corresponding diameters range from 6 to 11 nm, with size distributions on the order of ∼15%. Overall diameters are generally below twice the bulk exciton Bohr radius of CdTe (albeit in the intermediate to weak confinement regime), suggesting confinement effects in the linear absorption. Supporting this are clear blue shifts of the band edge, relative to the bulk band gap of CdTe (∼1.5 eV, ∼827 nm). Additional structure can also be seen at higher energies, implying the presence of

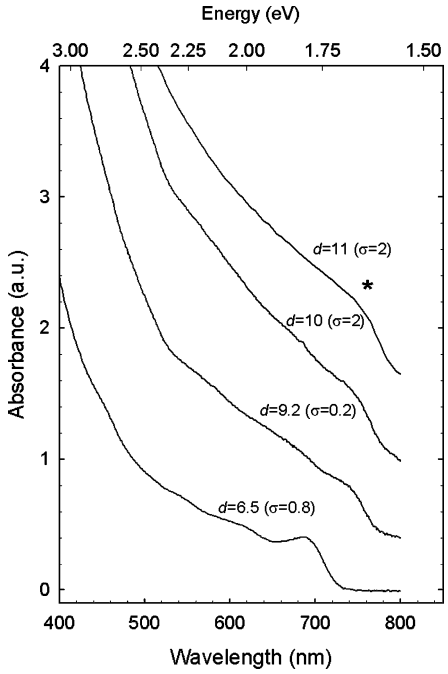


**Figure 10.** UV−vis absorption spectra of straight and branched CdTe NWs. The asterisk denotes a Se doped sample.

quantized sub-bands. For the smallest diameter NWs (bottom, Figure 10), both trends are readily apparent. In all cases, a simple "particle in a cylinder" model can be used to qualitatively estimate the various sub-band energies.[51]

To further explore the excited-state sub-band progression, transient differential absorption (TA) experiments were conducted on both straight and branched NWs (Figure 11). Previous TA studies on CdSe NWs have provided estimates of both interband and intraband relaxation rates as well as sub-band positions.[52] TA experiments were conducted on analogous CdTe NWs by exciting them at 387 nm (3.2 eV). At least two sub-bands labeled A and B were observed. For comparison, the solution linear absorption is superimposed over the TA data (Figure 11a). Depopulation of the higher energy subband, B, occurs very quickly (∼1 ps). This is slightly faster than that observed in analogous CdSe NWs where relaxation to the band edge occurs in approximately 3 ps.[52] At the band edge, A undergoes interband relaxation on a time scale of ∼3 ps, again faster than in CdSe (hundreds of picoseconds).[52] Since no band edge or deep trap emission is observed, a significant nonradiative component likely exists in the recovery. Furthermore, the low fluorescence quantum yield of the NWs prevents single wire absorption/emission polarization anisotropy measurements. Future polarization sensitive photoconductivity measurements (as done with CdSe)[39] may, however, yield more insight into these properties.

Additional experiments were undertaken to calculate relevant NW absorption cross sections ($\sigma$). Preliminary estimates, far to the blue of the band edge, were carried out as done previously.[53] Specifically $\sigma$ was modeled using the

(48) Jun, Y. W.; Lee, J. H.; Choi, J. Cheon, J. *J. Phys. Chem. B* **2005**, *109*, 14795.
(49) Mohamed, M. B.; Tonti, D.; Al-Salman, A.; Chemseddine, A.; Chergui, M. *J. Phys. Chem. B* **2005**, *109*, 10533.
(50) Dinega, D. P.; Bawendi, M. G. *Angew. Chem., Int. Ed.* **1999**, 38, 1788. Sun, S.; Murray, C. B. *J. Appl. Phys.* **1999**, *85*, 4325. Puntes, V. F.; Krishnan, K. M.; Alivisatos, A. P. *Science* **2001**, *291*, 2115.
(51) Gudiksen, M. S.; Wang, J. F.; Lieber, C. M. *J. Phys. Chem. B* **2002**, *106*, 4036.
(52) Robel, I.; Bunker, B. A.; Kamat, P. V.; Kuno, M. *Nano Lett.* **2006**, *6*, 1344.
(53) Protasenko, V. V.; Hull, K. L.; Kuno, M. *Adv. Mater.* **2005**, *17*, 2942.

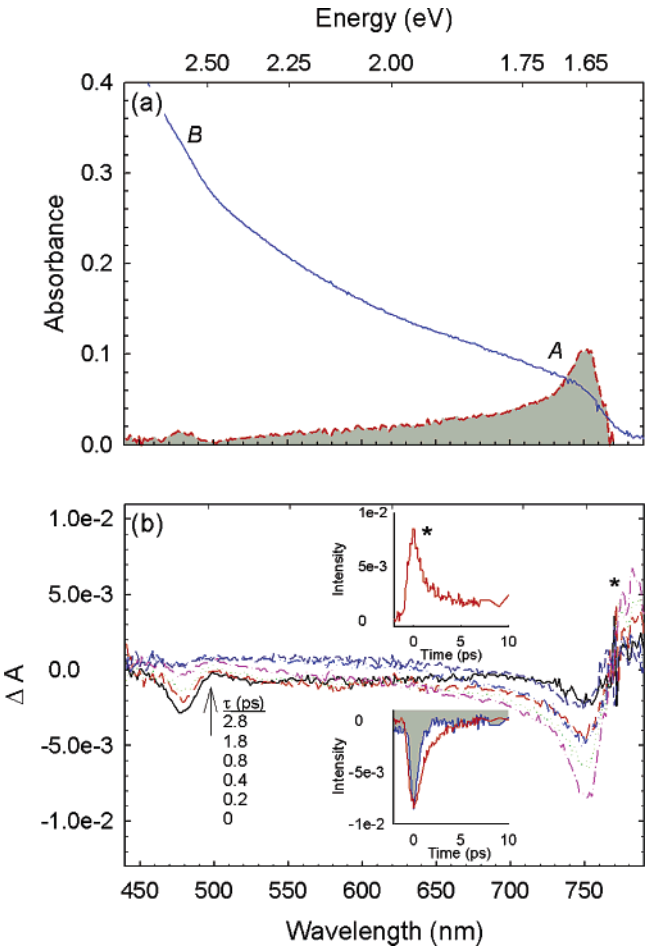


**Figure 11.** (a) Linear absorption and corresponding transient absorption spectrum 0.8 ps after excitation. (b) Differential transient absorption spectral plotted as a function of time. Top inset: kinetics of the induced absorption, denoted by an asterisk. Bottom inset: kinetics of both the band edge (shaded) and higher energy induced bleaches.

expression

$$\sigma(\mathrm{cm}^2) = \frac{\omega}{n_I c}(\pi r^2 l)\left|\frac{4\epsilon_I}{\epsilon_I + \epsilon_s}\right|^2 (2 n_s k_s) \qquad (1)$$

where $\omega$ is the angular frequency of the pump ($4.9 \times 10^{15}$) $s^{-1}$, $n_I$ is the refractive index of the surrounding medium (toluene, $n_I \sim 1.5$), $r$ is the NW radius (5 nm), $l$ is the length (5 $\mu$m), $\epsilon_I(\epsilon_s)$ is the dielectric constant of the surrounding medium (semiconductor) [$\epsilon_I \sim 2.2$, $\epsilon_s = (\epsilon_1 + i\epsilon_2) = 9 + i10$],[54] and $n_s(k_s)$ are the real (imaginary) parts of the semiconductor refractive index ($n_s \sim 3.4$, $k_s \sim 1.5$, derived from the standard relations $n_s = \sqrt{\epsilon_1 + \sqrt{\epsilon_1^2 + \epsilon_2^2}}(1/\sqrt{2})$, $k_s = \sqrt{-\epsilon_1 + \sqrt{\epsilon_1^2 + \epsilon_2^2}}(1/\sqrt{2})$. The resulting cross section at 387 nm is $\sigma_{387}(\mathrm{cm}^2) \sim 3 \times 10^{-10}$ cm$^2$ and is comparable to values obtained earlier for complementary CdSe NWs ($\sigma_{387\ \mathrm{nm}} \sim 1.1 \times 10^{-11}$ cm$^2$).[52]

Experimental cross sections were obtained by correlated ICPAES, linear absorption, and TEM measurements. ICPAES measurements were carried out by dissolving the NWs in 5% nitric acid. The concentrations of metal/chalcogen atoms were then determined relative to standardized solutions of Cd and Te. Typical Cd/Te concentrations ranged from $10^{-1}$ to $10^{-3}$ mmol/L, from which the total mass of CdTe was determined (typically $\sim 10^{-6}$ g in 1 cm$^3$ of solution). Dividing this value by the density of CdTe ($\rho = 5.85$ g/cm$^3$) and the physical area of a NW face (mean diameters derived from actual TEM measurements, typical area $\sim 5.8 \times 10^{-13}$ cm$^2$) gives the effective length of a single NW responsible for all of the mass in the ICPAES solution. Correlating this data to the linear absorption of samples enables one to extract an absorption "linear cross-sectional density" ($\chi$) in units of cm$^2$/$\mu$m. Typical values are $\chi \sim 1.96 \times 10^{-12}$ cm$^2$/$\mu$m at the band edge, $\chi \sim 8.00 \times 10^{-12}$ cm$^2$/$\mu$m at 488 nm (2.54 eV), and $\chi \sim 1.80 \times 10^{-11}$ cm$^2$/$\mu$m at 387 nm (3.20 eV). When the length of a typical NW is assumed (for example $\sim 1$ $\mu$m), a lower limit to its actual absorption cross-section (due orientational averaging) is obtained in good agreement to that predicted above. More specifically, a value of $3 \times 10^{-11}$cm$^2$ is obtained for a 1 $\mu$m, 10 nm diameter NW at 488 nm ($7.2 \times 10^{-11}$cm$^2$ at 387 nm). To account for orientational angle averaging, we explicitly consider the $\cos^2 \phi$ dependence of the absorbed light intensity,[55] where $\phi$ is the angle between the NW growth axis and the incident light polarization. When taken into account, the previous angle averaged cross sections increase by a factor of $\sim 3$ ($\sim 1.87 \times 10^{-11}$ cm$^2$ at 488 nm and $4.20 \times 10^{-11}$ cm$^2$ at 387 nm).

To complete our survey of relevant NW optical/electrical properties, general "ballpark" electrochemical band offsets were estimated using cyclic voltammetry.[56] Experiments were conducted on both CdTe and CdSe NWs for comparison purposes. In both cases, NWs were dispersed onto platinum electrodes and were allowed to dry. Acetonitrile and tetrabutylammonium perchlorate were used as a solvent and electrolyte, respectively. Experimental scan rates were varied from 10 to 50 mV/s. Resulting peak currents were proportional to this rate, showing that the observed currents originate from the electrochemical reduction/oxidation of the NWs. Representative cyclic voltammograms for both CdTe and CdSe NWs as well as for the solvent itself are provided in the Supporting Information. More details about the peak assignments are also provided in the Supporting Information.

For CdTe an anodic (cathodic) peak is observed at 0.89 V (−0.82 V). Furthermore, the potential difference (1.71 V) between these peaks is consistent with the optical band gap of the sample, suggesting that the anodic (cathodic) peak is related to the oxidation (reduction) potential of the wires. In turn, this provides a measure of the NW electron affinity (3.62 eV) and ionization potential (5.33 eV). The same behavior is observed with CdSe where an anodic (cathodic) peak is observed at 0.85 V (−0.97 V). Corresponding values for the electron affinity and ionization potential are 3.47 and 5.29 eV, respectively. Their difference (1.82 V) is also in good agreement with the optical band gap of the sample. Finally, on comparing the CdTe and CdSe data, these

(54) Marple, D. T. F.; Ehrenreich, H. *Phys. Rev. Lett.* **1962**, *8*, 87.

(55) Zhou, R.; Chang, H-C.; Protasenko, V.; Kuno, M.; Kumar, A.; Jena, D, Xing, H. Submitted.

(56) Haram, S. K.; Quinn, B. M.; Bard, A. J. *J. Am. Chem. Soc.* **2001**, 123, 8860. Kucur, E.; Riegler, J.; Urban, G. A.; Nann, T. *J. Chem. Phys.* **2003**, *119*, 2333. Querner, C.; Reiss, P.; Sadki. S.; Zagorska, M.; Pron, A. *Phys. Chem. Chem. Phys.* **2005**, *7*, 3204. Poznyak, S. K.; Osipovich, N. P.; Shavel, A.; Talapin, D. V.; Gao, M.; Eychmuller, A.; Gaponik, N. *J. Phys. Chem. B* **2005**, *109*, 1094.

(preliminary) results reveal general, order of magnitude, band offsets between the two materials. Specifically, a 15 meV (40 meV) offset appears to exist between their conduction (valence) bands (Supporting Information). As such, the wires appear to exhibit type-II behavior predicted for CdSe relative to CdTe.

## Conclusions

High quality straight and branched CdTe NWs have been synthesized via a solution-based, solution−liquid−solid approach. Low melting Au/Bi nanoparticles were used to induce 1D nanowire growth. Resulting straight CdTe NWs have narrow diameters and lengths exceeding 10 $\mu$m in many cases. Size distributions of as made ensembles are on the order of 15% with corresponding intrawire diameter distributions of ∼5%. Branched NWs were made by varying straight NW reaction conditions. In particular, the temperature and metal/chalcogen stoichiometry were found to play an important role in dictating branching. Resulting branched NW morphologies include tripod, v-shape, y-shape, merge-y, and higher order structures. ZB/W phase admixtures in the wires are suggested as being primarily responsible for the phenomenon since the central branching point of each wire is a triangular ZB core with four equivalent {111} faces. In all cases, confinement effects are observed in the NW linear absorption. These effects appear as blue shifts of the band edge relative to the bulk band gap and by the presence of structure at higher energies. Typical absorption cross sections are $\sim 10^{-12}$ cm$^2$ at the band edge, $7 \times 10^{-12}$ cm$^2$ at 488 nm, and $\sim 10^{-11}$ cm$^2$ at 387 nm. The NWs therefore absorb strongly, with cross sections nearly 5 orders of magnitude larger than those of complementary QDs.[57] Preliminary transient differential absorption measurements, as well as electrochemical studies, have provided estimates of relevant intra/interband relaxation rates, higher energy sub-band positions, and conduction/valence band offsets. In particular, preliminary TA studies show fast intraband relaxation to the band edge within 1 ps and a similarly rapid 3 ps interband decay. The latter is consistent with the low fluorescence quantum yield of the NWs.

Additional studies are suggested by the current study. For example, a more thorough Rietveld analysis of the phase admixture in CdTe can be conducted in future studies by fitting powder X-ray diffraction spectra to contributions from crystallographic texture as well as ZB/W phase admixtures. This may confirm the temperature-dependent nucleation of ZB over W and may, in turn, suggest ways for better achieving nanowire shape control. From an optical standpoint, more thorough studies of the linear absorption cross sections of these NWs are suggested. Furthermore, polarization sensitive photoconductivity measurements may eventually enable an investigation of the polarization anisotropy of these wires given the absence of band edge emission. In all cases, the high quality of the resulting wires, their narrow diameters, size distributions, and large absorption cross sections suggest potential uses in photovoltaic and/or polarization sensitive devices.

**Acknowledgment.** We thank the University of Notre Dame, the Notre Dame Faculty Research Program, the ACS Petroleum Research Fund, the Notre Dame Radiation Laboratory, and the Office of Basic Energy Sciences of the U.S. Department of Energy for financial support and for use of their facilities. We thank Istvan Robel for assistance with the femtosecond transient absorption experiments. We thank Anusorn Kongkanand for assistance with the cyclic voltammetry measurements. M.K. also thanks the National Science Foundation for a NSF CAREER award in support of this work. M.K. is a Cottrell Scholar of Research Corporation.

**Supporting Information Available:** Additional low-resolution TEM micrographs of straight and branched CdTe NWs. High-resolution TEM images of straight NWs. High-resolution TEM images of catalyst particles attached to NW ends. Energy dispersive X-ray spectrum of straight CdTe NWs. Cartoon scheme illustrating general growth directions of straight and branched NWs as well as common imaging directions in TEM experiments. Additional high-resolution TEM images of branched CdTe NWs. Low-resolution TEM images of higher order CdTe NWs. High-resolution TEM images of Se-doped tripod CdTe NWs. Electrochemical cyclic voltammograms of CdSe and CdTe NWs. Estimated band offsets between CdSe and CdTe NWs. This material is available free of charge via the Internet at http://pubs.acs.org.

CM061559M

(57) Yu, W. W.; Qu, L. H.; Guo, W. Z.; Peng, X. G. *Chem. Mater.* **2003**, *15*, 2854.